International Journal of Microwave and Wireless Technologies

cambridge.org/mrf

Bi-layered/tri-layered bio-media in direct contact with metal diagonal horn for hyperthermia

Soni Singh, Bhagirath Sahu and S. P. Singh

Department of Electronics Engineering, Indian Institute of Technology (BHU), Varanasi, UP 221 005, India

Research Paper

Cite this article: Singh S, Sahu B, Singh SP (2018). Bi-layered/tri-layered bio-media in direct contact with metal diagonal horn for hyperthermia. *International Journal of Microwave and Wireless Technologies* **10**, 921–932. https://doi.org/10.1017/S1759078718000739

Received: 12 October 2017
Revised: 12 April 2018
Accepted: 13 April 2018
First published online: 11 May 2018

Key words:
Bi-layered/tri-layered bio-media; hyperthermia; metal diagonal horn; specific absorption rate; thermal analysis

Author for correspondence: S. P. Singh, E-mail: spsingh.ece@iitbhu.ac.in

Abstract

In this paper, theoretical/simulation study of specific absorption rate (SAR) and/or temperature distributions in a bi-layered bio-media (fat and muscle)/realistic tri-layered bio-media (skin, fat, and muscle layers) in direct contact with water-loaded metal diagonal horn (MDH) designed at 915 MHz are investigated. The effects of fat thickness on the input reflection coefficient, reflection coefficient at the interface between the MDH and the bi-layered bio-media, and the SAR distribution in the bi-layered bio-media are also studied through simulation and theoretically at 915 MHz. Further, the SAR parameters such as penetration depth and effective field size inside the bi-layered bio-media due to the MDH are evaluated theoretically and the theoretical results are compared with the corresponding simulation results. Finally, SAR and temperature distributions in tri-layered bio-media without and with embedded irregular/oval-shaped tumor are provided for demonstrating the hyperthermia performance of the MDH applicator.

Introduction

Hyperthermia is used for cancer therapy. Clinical results demonstrated that temperature in the range of 41–45 °C is needed for hyperthermia, but care should be taken to keep the temperature of surrounding healthy tissue below 41 °C. The effect of the thickness of fat overlying the muscle layer is an important aspect of research for microwave hyperthermia. The fat layer behaves like a shielding structure due to much smaller conductivity and dielectric constant than muscle layer, and hence restricts microwave to effectively penetrate into the muscle tissue to heat the tumors [1]. Also, the large thickness of fat layer causes less power to reach the muscle tissue region and hence less heating of the muscle tissue, which necessitates higher power to be fed to the applicator for effective hyperthermia. The effect of fat thickness on the heating pattern of the microwave applicator is investigated in reference [2, 3]. Various applicators terminated in planar fat-muscle phantom are reported in the literature, for example, multimodal applicator [4], Lucite-cone waveguide applicator [5], and rectangular aperture source [6]. In reference [6], theoretical expressions for electromagnetic (EM) fields and associated heating pattern in layered biological tissue due to a rectangular aperture source are reported, in which the source generates linearly polarized aperture field distribution. Further, circularly polarized and implantable antennas are also reported for bio-medical applications [7, 8].

Since the induced field distribution and heating pattern in inhomogeneous bi-layered media due to exposure of the media to near field of the applicator are complicated functions of many bio-media and applicator parameters, it is very important to study the effects of fat thickness on the interface reflection parameters and specific absorption rate (SAR) distribution in the bio-media for hyperthermia applications. Treatment quality can be optimized with the help of EM and thermal simulators. Thermal simulation can be performed for achieving desired temperature distribution as well as optimizing heating of tumor compared with normal tissue [9].

Recently, Singh and Singh [10, 11] demonstrated the characteristics of water-loaded metal diagonal horn (MDH) in direct contact with homogeneous muscle-medium for hyperthermia application. In realistic hyperthermia applicator, muscle along with skin and fat layers is present. Tri-layered skin-fat-muscle tissue models with fixed layer thicknesses have provided further details in an effort to approach towards realistic scenario but do not quantify the effects for a range of fat layer thickness in human tissue [12, 13]. It is to be noted that the study of the effect of fat thickness on the applicator's characteristic is very important. Hence, the present study focuses on the theoretical computation of SAR distributions in the planar fat-muscle bi-layered phantom owing to water-loaded MDH, and other antenna related parameters at industrial, scientific, and medical (ISM) frequency of 915 MHz. Additionally, to visualize the hyperthermia performance of the applicator, simulations were performed in which the tri-layered bio-media without and with the embedded tumor is in direct contact with the applicator. To the best of the authors' knowledge, no theoretical and/or simulation work

CAMBRIDGE UNIVERSITY PRESS

has been done on water-loaded MDH demonstrating the effect of fat thickness on the characteristic of hyperthermia applicator.

The objectives of the present paper are to investigate, theoretically/through simulation, the SAR and/or temperature distributions in the phantom bi-layered bio-media (fat and muscle layers)/tri-layered bio-media (skin, fat, and muscle layers) with direct-contact water-loaded MDH at 915 MHz for hyperthermia. The effects of fat thickness on the input reflection coefficient/reflection coefficient at the interface between the MDH and bi-layered media, applicator's aperture admittance and the peak SAR in the muscle layer are also studied through simulation and/or theoretically at 915 MHz. The plane wave spectral technique is employed for theoretical analysis. The heating process is simulated using EM and thermal solver. For EM simulations, CST Microwave studio (MWS) software is used while CST Multi-physics software is employed for thermal simulations [14].

Design and theory

Applicator design

The design procedure given by Love [15] for empty horn terminated in free space and given in reference [11] for water-loaded MDH terminated in homogeneous muscle medium was adopted to achieve water-loaded MDH terminated in bi-layered media (fat and muscle) at ISM frequency of 915 MHz. For the sake of brevity, the detailed design procedure of the present antenna is not reported here. The optimized dimensions of the MDH antenna designed at 915 MHz are given in Figs 1(a) and 1(b). The structure of water-loaded MDH terminated in bi-layered bio-media is shown in Fig. 1(c). The conducting ground plane of size 250×250 mm^2 is used in xy-plane of the aperture of the antenna for significant suppression of fringing electric field.

Theory

Analysis of field components inside the bi-layered media (Fat and muscle layers)

The analysis of fields in bi-layered media is carried out using the plane wave spectral technique discussed by Compton [16] and Harrington [17]. Recently, the induced field components in homogeneous muscle medium due to known field distributions at the apertures of water-loaded MDHs designed at 915 and 2450 MHz was determined using plane wave spectral technique [11]. In the present paper, the plane wave spectral technique has been employed to theoretically evaluate the induced field components in an inhomogeneous two-layered bio-media (fat and muscle) due to the water-loaded MDH designed at 915 MHz. In the present analysis, the fat layer is assumed to be of finite thickness "t_2" followed by an infinite muscle layer. Fat and muscle layers have complex relative permittivities of ε_1^* and ε_2^* respectively. Reference [11] can be referred for the detailed analysis of induced field components in the homogeneous muscle medium due to MDH.

The x-, y-, and z-components of electric and magnetic fields in the i^{th} inhomogeneous bio-layer ($i = 1$ for fat layer and $i = 2$ for muscle layer) and hence, the electric field induced in the bi-layered bio-media (fat and muscle layers) due to the applicator are determined as given in the reference [11, 16] for homogeneous bio-medium.

The resultant electric field intensity in the i^{th} biological layer is given by

$$|E_i|^2 = |E_{x_i}|^2 + |E_{y_i}|^2 + |E_{z_i}|^2, \tag{1}$$

where E_{x_i}, E_{y_i}, and E_{z_i} are the x-, y- and z- components of the induced electric field in the i^{th} biological layer.

The SAR in the i^{th} biological layer ($i = 1, 2$) can be evaluated by

$$\text{SAR} = \frac{\sigma_i |E_i|^2}{2\rho_i}, \tag{2}$$

where σ_i and ρ_i are the conductivity and density of i^{th} biological layer respectively, and $|E_i|$ is the magnitude of total induced electric field strength inside the i^{th} biological layer.

Aperture admittance and reflection coefficient at the interface between the antenna aperture and bi-layered bio-media

The aperture admittance [11, 16] of the MDH terminated in phantom bi-layered (fat and muscle) bio-media is given by

$$Y_A = \int_{-d/2}^{d/2} \int_{-d/2}^{d/2} \left\{ \vec{E}_{x1}(x, y, 0).\vec{H}^*_{y1}(x, y, 0) - \vec{E}_{y1}(x, y, 0).\vec{H}^*_{x1}(x, y, 0) \right\} dx dy, \tag{3}$$

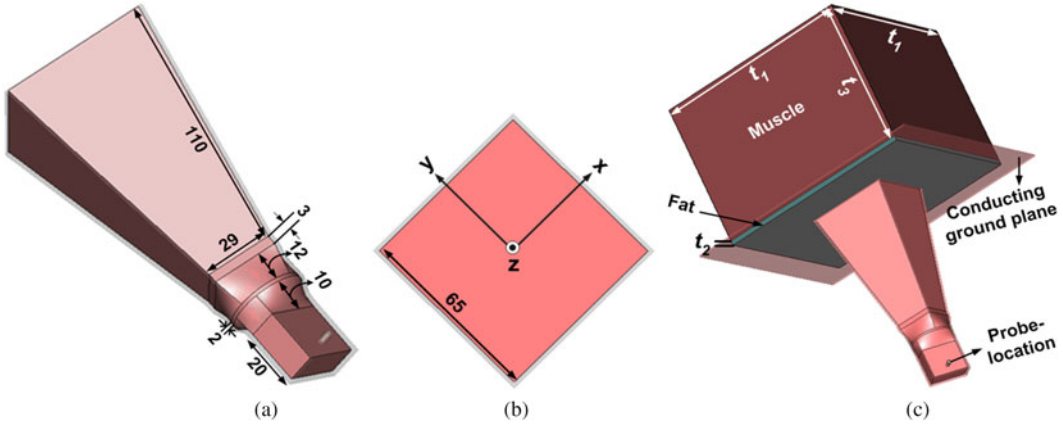

Fig. 1. Geometry of MDH (a) 3-D view (b) front view (c) terminated in a bi-layered bio-media (all dimensions are in mm).

https://doi.org/10.1017/S1759078718000739 Published online by Cambridge University Press

Table 1. Dielectric properties of bio-media [18]

Tissue type (*i*)	ε_r	Density (kg/m^3)
Fat (1)	11.3–j2.16	920
Muscle (2)	55–j19	1050

where $\overrightarrow{E}_{x1}(x, y, 0)$, $\overrightarrow{E}_{y1}(x, y, 0)$ and $\overrightarrow{H}^*_{x1}(x, y, 0)$, $\overrightarrow{H}^*_{y1}(x, y, 0)$ are the x and y components of electric and magnetic fields at the MDH aperture ($z = 0$) respectively, and d (=65 mm) is the aperture dimension of the MDH designed at 915 MHz.

Reflection occurs due to changes in physical properties at the interface of MDH and fat-layer. Therefore, reflection coefficient at the interface can be written as

$$\Gamma = \frac{Z_A - Z_0}{Z_A - Z_0}, \tag{4}$$

where Z_A (=$1/Y_A$) is the impedance at the MDH aperture, Z_0 is the characteristic impedance of the MDH [11].

Results and discussion

Applicator's characteristics and SAR distributions in bi-layered bio-media

The theoretical variations of aperture admittance and reflection coefficient at the interface between the MDH antenna and the fat layer, and normalized SAR distributions in the bi-layered bio-media (fat and muscle layers) for fat thickness (t_2) of 5 mm were obtained at 915 MHz by solving the equations given in the section "Design and theory" using MATLAB software. In the present investigation, muscle layer is assumed to be of infinite thickness. The applicator's design data along with dielectric properties and density of phantom bi-layered bio-media (fat-muscle media) given in reference [11], Table 1 and Fig. 1 have been used to obtain the theoretical and simulated SAR distributions. The theoretical variations of aperture admittance and reflection coefficient at the interface between the MDH and fat layer versus fat thickness were determined using equations (3) and (4) and the results are illustrated in Fig. 2. The variation of reflection coefficient obtained at the interface between the MDH aperture and fat layer (that is dependent upon aperture as well as characteristic admittances of the MDH) with fat thickness indicates that as the thickness of fat layer increases, impedance matching between the MDH aperture and the fat layer becomes progressively worse.

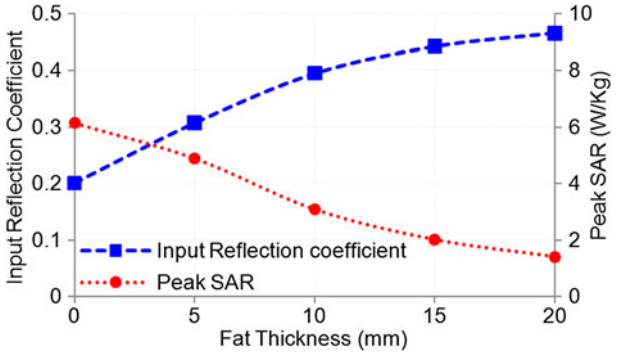

Fig. 3. Variations of simulated input reflection coefficient for the MDH and peak SAR inside the muscle layer as functions of fat thickness.

The theoretical results for normalized SAR distribution in the bi-layered bio-media due to the MDH evaluated at 915 MHz using equations provided in the section "Design and theory" are given in Fig. 4.

The simulated variations of input reflection coefficient and peak SAR in the muscle layer of phantom bi-layered bio-media of cross section $t_1 \times t_1 = 200 \times 200$ mm^2 as functions of fat thickness, and normalized SAR distribution in the bi-layered bio-media for fat thickness (t_2) of 5 mm and muscle thickness (t_3) of 150 mm (for which input reflection coefficient was found to be 0.3077 (=−10.2 dB)) owing to the water-loaded applicator designed at 915 MHz were determined using CST MWS software and the simulation results are shown in Figs 3 and 4, respectively. Initially, 1 W power fed to the antenna was taken in the simulation study. The SAR values are normalized with respect to the maximum value of SAR in the muscle layer. As the SAR value beyond 60 mm in muscle region is negligible at the design frequency of 915 MHz, muscle thickness $t_3 = 150$ mm taken in simulation study is equivalent to an infinitely thick bio-medium.

It is apparent from Fig. 3 that as the fat thickness increases, the effective relative permittivity of the bi-layered bio-media becomes less, and hence the impedance matching at the interface between the aperture of the MDH and the effective bi-layered bio-media deteriorates, which increases the reflection coefficient at the interface, and hence, the input reflection coefficient also. Peak SAR value in muscle layer reduces as interface reflection is increased with fat thickness.

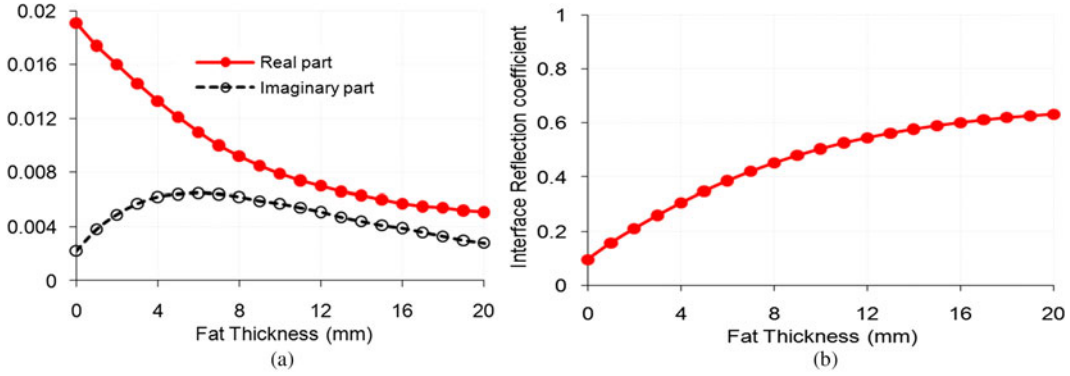

Fig. 2. Variations of theoretical (a) aperture admittance (b) reflection coefficient at the interface of the MDH and bi-layered tissue as functions of fat thickness.

https://doi.org/10.1017/S1759078718000739 Published online by Cambridge University Press

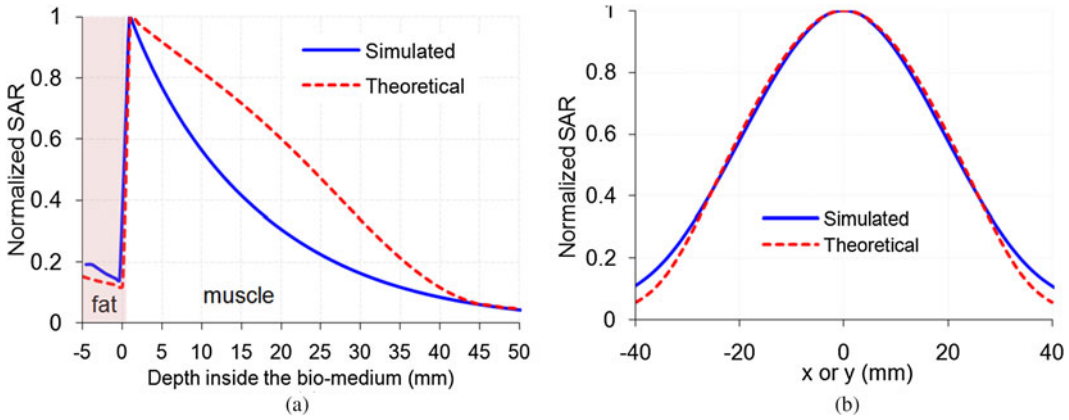

Fig. 4. Normalized SAR distributions inside the bi-layered bio-media due to MDH along (a) *z*-direction (b) *x*-/*y*-direction at $z = 10$ mm.

Table 2. SAR parameters inside the muscle medium due to the MDH antenna at 915 MHz (fat thickness $t_2 = 5$ mm)

Tissue type	Penetration depth (mm)		Effective field size (mm^2)	
	Simulated	Theoretical	Simulated	Theoretical
Muscle medium[a]	36	39	46 × 46	44 × 44
Fat-muscle	33	36	44 × 44	44.5 × 44.5

[a]Corresponds to homogeneous muscle medium only.

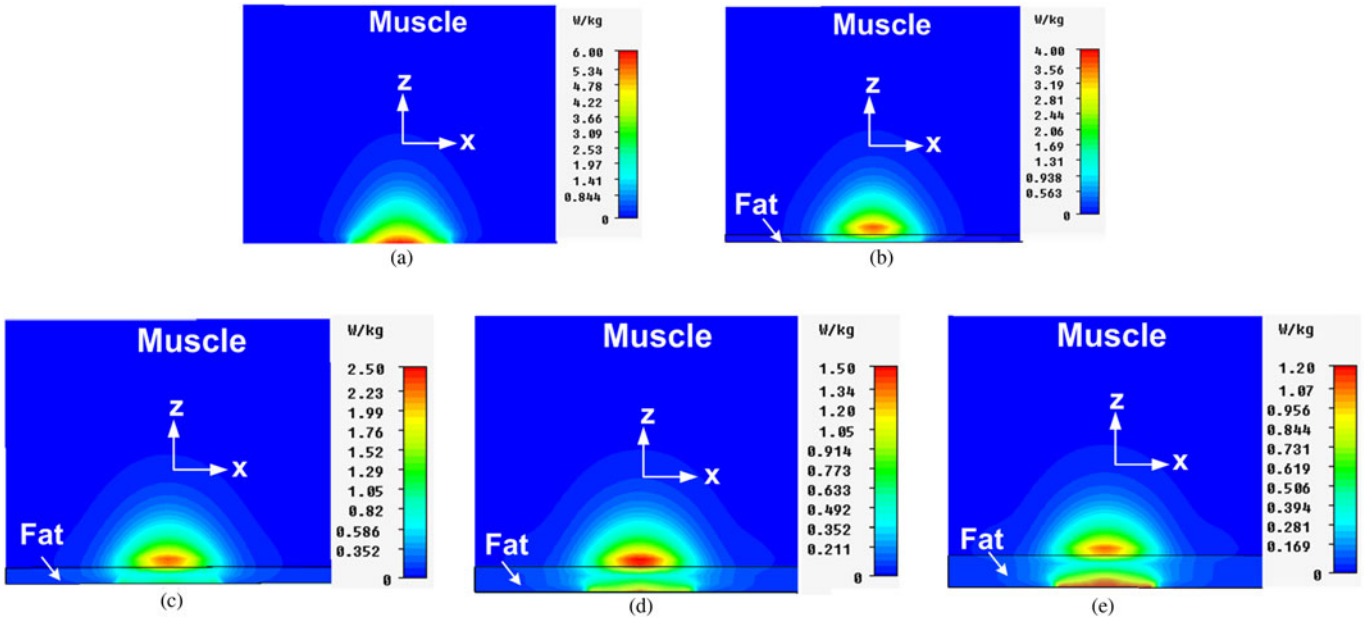

Fig. 5. Simulated SAR distributions inside the bi-layered bio-media due to the MDH for different values of fat thickness (a) $t_2 = 0$ mm (b) $t_2 = 5$ mm (c) $t_2 = 10$ mm (d) $t_2 = 15$ mm (e) $t_2 = 20$ mm.

Figure 4(a) shows the normalized SAR distribution in the inhomogeneous bi-layered media in *z*-direction due to the MDH. The values of simulated and theoretical penetration depth (depth where SAR value is down to 13.5% of the maximum in the muscle) extracted from Fig. 4(a) are given in Table 2 for the antenna designed at 915 MHz. The normalized SAR distributions along *x*-/*y*-direction in the muscle layer due to the MDH designed at 915 MHz are depicted in Fig. 4(b). The values of simulated and theoretical effective field size (EFS), which is defined as the area enclosed within 50% SAR contour inside the phantom bio-medium are extracted from Fig. 4(b) and the results are listed in Table 2. It can be seen from Fig. 4 and Table 2 that the

https://doi.org/10.1017/S1759078718000739 Published online by Cambridge University Press

Table 3. Proposed MDH parameters at 915 MHz (fat thickness $t_2 = 5$ mm)

Parameter	Proposed MDH in direct contact with bi-layered bio-media (separation = 0 mm)	MDH in close proximity with bi-layered bio-media		
		Separation = 1 mm	Separation = 3 mm	Separation = 5 mm
Input reflection coefficient (dB)	−10.2	−8.66	−7.189	−6.39
Peak SAR (W/kg)	4	3.2	1.8	1.1

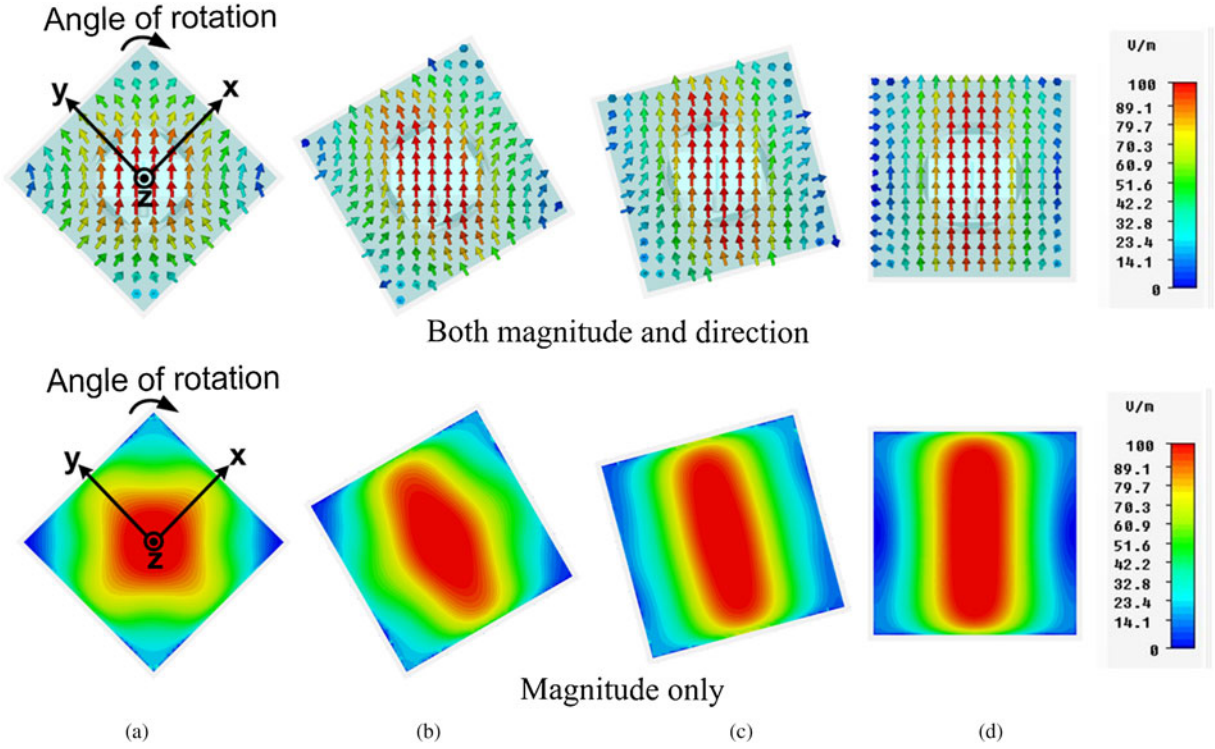

Fig. 6. Electric field distributions at the antenna aperture for different angles of rotation of polarization vector with respect to aperture diagonal (a) 45° (proposed MDH), (b) 30°, (c) 15°, (d) 0° at 915 MHz.

Table 4. Effect of rotation angle of polarization vector (with respect to diagonal of antenna aperture) on peak SAR and input reflection coefficient at 915 MHz

Rotation angle (°)	Peak SAR (W/kg)	Input reflection coefficient (dB)	EFS (mm × mm)
45 (Proposed antenna)	4	−10.20	44 × 44
30	3.9	−10.09	52 × 38
15	3.7	−9.44	58 × 34
0	3.7	−9.57	59 × 33

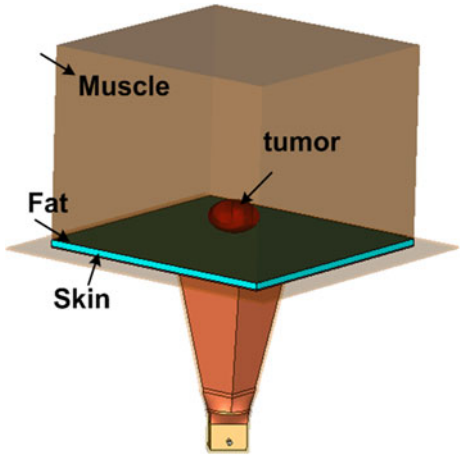

Fig. 7. Structure of MDH antenna terminated in tri-layered bio-media with embedded tumor.

simulated and theoretical results are almost in agreement. Hence, close agreement between theoretical and simulated results proves the validity of plane wave spectral technique which provides theoretical SAR distribution. The little variation in the theoretical and simulated results may be due to the approximations made in the theoretical analysis.

Figure 5 depicts the results for simulated SAR distribution results in the bi-layered bio-media for different fat thicknesses. From Fig. 5, the following observations can be made: for thin fat layer, the effective dielectric constant of the bi-layered bio-media is higher which results in reduced interface reflection. Since muscle layer forms a major part of the effective bio-

https://doi.org/10.1017/S1759078718000739 Published online by Cambridge University Press

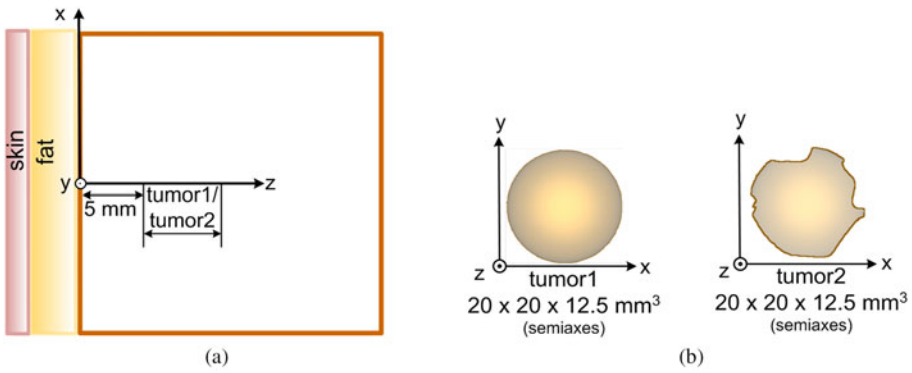

Fig. 8. (a) Two-dimensional realistic tri-layered bio-model with embedded tumor1/tumor2, and (b) Enlarged view of tumor1/tumor2.

Table 5. Properties of tri-layered bio-media and tumor [18]

Tissue/Tumor	Thickness (mm)	Density (kg/m^3)	ε_r
Skin	1	1130	46–j16.7
Fat	5	920	11.3–j2.16
Muscle	80	1050	55–j19
Tumor1/Tumor2	25	1050	58–j21.6

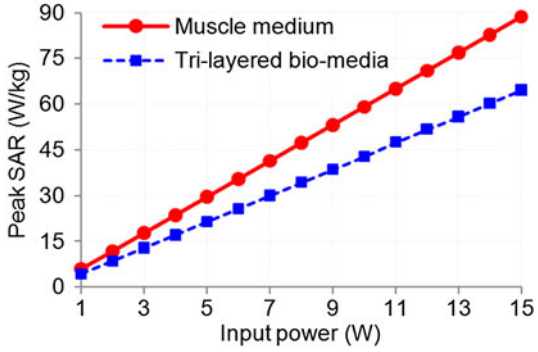

Fig. 9. Variations of peak SAR with input power.

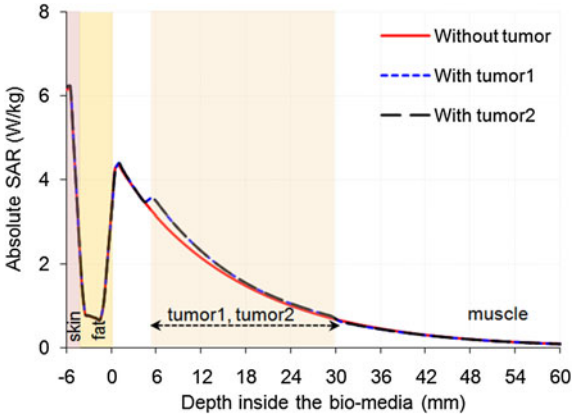

Fig. 10. Simulated absolute SAR distributions inside the tri-layered bio-model without and with embedded tumor along z-direction ($x = y = 0$) due to the MDH for 1 W input power.

medium, SAR in muscle layer is high. But when fat thickness is sufficiently increased, the reflections at the interfaces of the muscle-fat layer and MDH aperture-fat layer become significant, which shifts the focusing spot of SAR from muscle layer to fat layer (Figs 5(d) and 5(e)).

It can be observed from Table 2 that presence of 5 mm thick fat layer reduces the penetration depth to reasonable extent whereas the change in the value of EFS is insignificant. This may be due to the significant reflections at the interfaces of antenna aperture-fat layer and fat-muscle layers because of great differences in the dielectric properties of water and fat layer as well as fat and muscle layers and in the impedances at corresponding interfaces.

Effect of proposed MDH-tissue separation on hyperthermia characteristics

The proposed MDH is in direct contact with inhomogeneous bi-layered bio-media. Direct contact applicators are more desirable as compared with spaced applicators because they reduced leakage (unwanted radiation). In order to study the effect of separation between the proposed MDH and tissue on input reflection coefficient and peak SAR at 915 MHz, simulations were conducted for four values of antenna-tissue separation (0, 1, 3, and 5 mm) and the results are given in Table 3. It is clear from Table 3 that as we increase the antenna-tissue separation, the value of peak SAR in the phantom muscle medium reduces since the coupling between the antenna and phantom reduces. However, the value of input reflection coefficient increases with antenna-tissue separation. As the separation between the antenna and tissue increases, the impedance matching between the antenna and tissue deteriorates since the larger thickness of the medium (free space) having a dielectric constant of 1 is interposed between the two media having much higher dielectric constant as compared with free space medium.

Polarization effect of the proposed MDH on hyperthermia characteristics

The proposed MDH is a diagonal horn antenna in which the mode of propagation within the horn is principally such that the electric vector is parallel to one of its diagonals when the electric field is excited diagonally, and hence it is referred to as diagonal horn. Hence, the proposed MDH is a diagonally polarized horn antenna. The 3-D view of the proposed MDH is shown in Fig. 1. It can be observed from Fig. 1 that standard rectangular waveguide carrying TE_{10} mode is gradually transformed to circular waveguide carrying the TE_{11} mode. Another gradual transition converts the circular cross-sections into the square, and the horn

https://doi.org/10.1017/S1759078718000739 Published online by Cambridge University Press

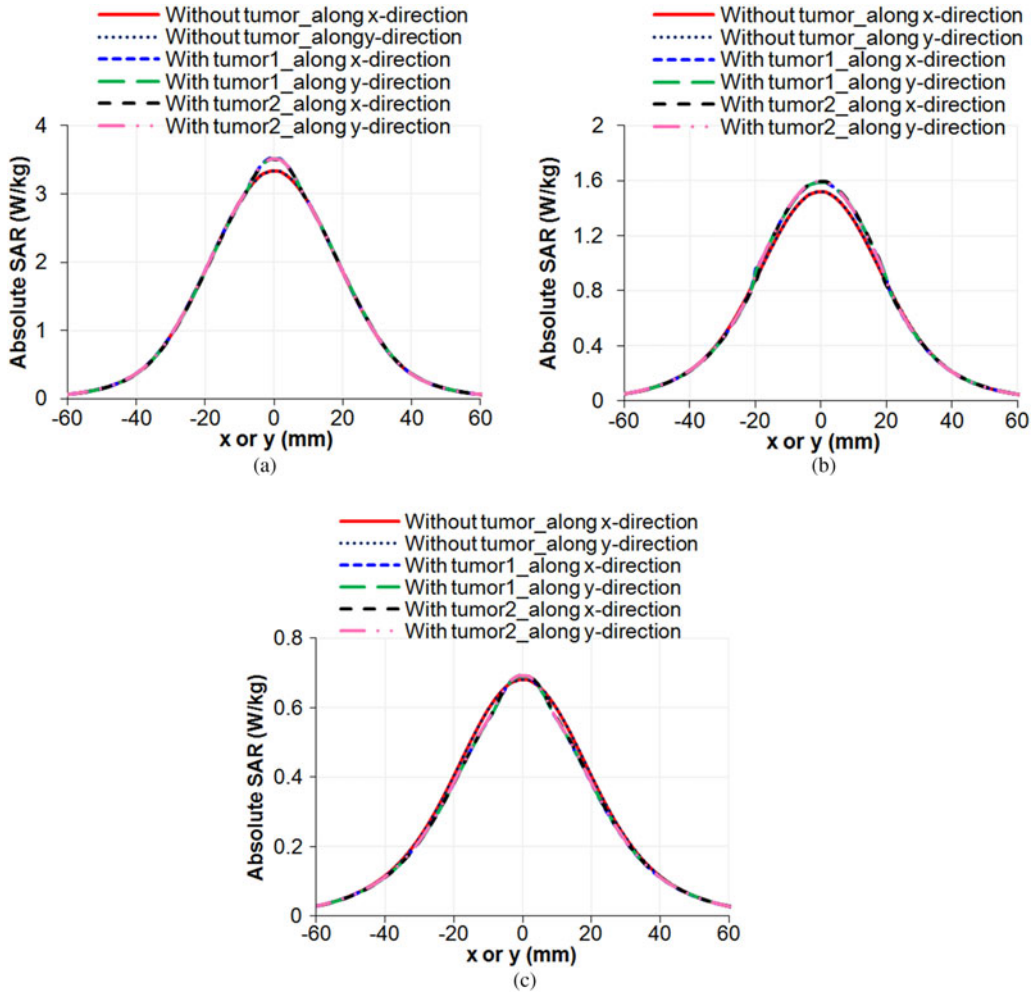

Fig. 11. Simulated absolute SAR distributions inside the tri-layered bio-model without tumor, with embedded tumor1 and with embedded tumor2 along *x*-/*y*-direction ($y/x = 0$) due to the MDH for 1 W input power at (a) $z = 5$ mm (b) $z = 17.5$ mm (c) $z = 30$ mm.

Table 6. Hyperthermia performance due to the proposed water-loaded MDH

Frequency	Tissue type	PD (mm)	EFS[$] ($mm^2$)	Depth at ΔT/2 (mm)	Heating area[a] {41–45 °C} (mm^2)
915 MHz	Without tumor	32.93	44.6 × 44.6	32	31.7 × 31.7
	With tumor1	32.92	42.5 × 42.5	34	42.16 × 42.16
	With tumor2	32.92	42.1 × 42.1	34	40.84 × 40.84

[a]EFS and heating area are defined in the middle of tumor.

Table 7. Thermal parameters of tri-layered bio-media and tumor1/tumor2 for the BHE [21, 22]

Tissue type	ρ (Kg/m^3)	C (KJ/Kg°C)	K (W/m°C)	A_0 (W/m^3)	B (W/m^3 °C)
Skin	.0.42	.3.5	.0.42	.1620	.9100
Fat	920	2.5	0.25	300	1700
Muscle	1050	3.6	0.5	480	2700
Tumor1/Tumor2	1050	3.6	0.5	480	675

then flares out to the desired aperture size. All the cross-sections of the proposed antenna are square including the aperture. It is clear from Fig. 1 that both square waveguide and aperture cross-sections are rotated by 45° with respect to the input rectangular waveguide. The two diagonals of the output opening (of square cross-section) of the circular-to-square transition coincide with the corresponding diagonals of the square waveguide and the antenna aperture. Due to this configuration, the wave which

https://doi.org/10.1017/S1759078718000739 Published online by Cambridge University Press

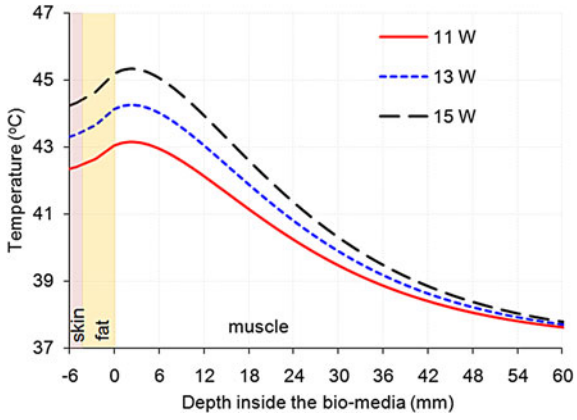

Fig. 12. Temperature distribution inside the tri-layered bio-media without tumor for different input power levels along *z*-direction ($x = y = 0$) due to the MDH.

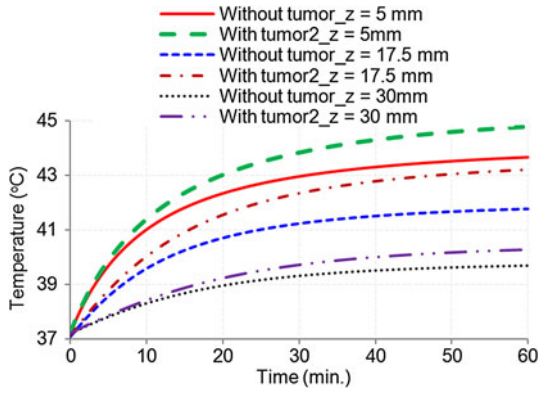

Fig. 13. Variations of temperature in the realistic tri-layered bio-media without and with embedded tumor2 versus time due to the MDH by taking depth in the tumor as a parameter for $x = y = 0$.

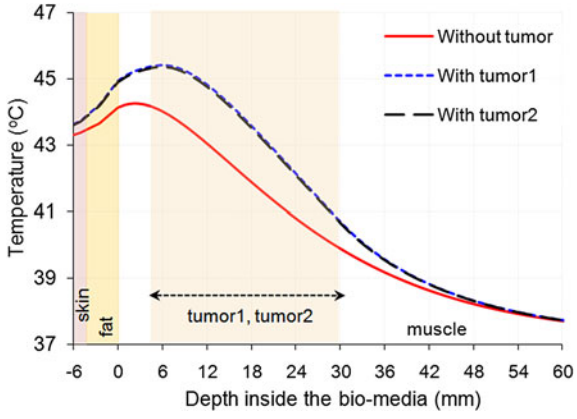

Fig. 14. Simulated temperature distributions inside the tri-layered bio-models without and with embedded tumor1/tumor2 along z-direction ($x = y = 0$) due to the MDH for 13 W optimum input power at 915 MHz.

propagates in the slowly flaring proposed horn is composed of two equal amplitude and equi-phase conventional modes (TE_{10} and TE_{01}) appropriate to the square waveguide. The electric field vector distribution at the aperture of the proposed MDH which is in direct contact with inhomogeneous bi-layered bio-media is shown in Fig. 6(a). It can be observed from Fig. 6(a) that distributions of E-fields are along the diagonal at the aperture of the horn. Further, the electric field distribution over the aperture of the proposed horn is identical in *E*- and *H*-planes, resulting in circularly symmetric field distribution.

In order to observe the polarization effect of the proposed MDH, the portion of the antenna structure of square cross-section is rotated for different angles with respect to input rectangular waveguide and the results for different rotation angles are given in Table 4. It is clear from Table 4 that as the angle of rotation changes, the polarization vector with respect to its aperture diagonal changes (Fig. 6), due to which the values of peak SAR, EFS and input reflection coefficient are altered (Table 4). Although little changes in the values of input reflection coefficient and peak SAR for different rotation angles are observed, however circularly symmetric EFS in the muscle region due to the proposed MDH is converted into elliptical distribution as the rotation angle for the polarization vector changes with respect to aperture diagonal of the proposed horn. Due to circularly symmetric field distribution, the proposed horn is a better choice for treatment of localized spherical (or near spherical) tumors in superficial region of the body.

SAR distributions in tri-layered bio-media

The performance of the MDH applicator is investigated through simulation for three tri-layered bio-models (one without tumor, and the other two consisting of superficial oval-and irregular-shaped abdominal/limb tumors) lying inside the muscle tissue taken one at a time as shown in Fig. 7. The locations of the oval- and irregular-shaped tumors embedded within second and third tri-layered bio-models are provided in Fig. 8(a). In all, two tumors of different shapes (tumor1 is of oval-shaped and tumor2 is of irregular-shaped) were considered in the present study (Fig. 8(b)).

For heating of tumors designated as tumor1 and tumor2, water-loaded MDH antenna designed at 915 MHz which is in direct contact with tri-layered bio-media containing the aforesaid tumors (one at a time) was considered. A cancerous tissue has higher water content [19] compared with healthy tissue, and hence higher dielectric constant and conductivity. The size and dielectric properties of tumors are given in Fig. 8/Table 5.

The absolute value of peak SAR in the bio-model is dependent on input power, tissue composition and frequency for the given wave polarization and applicator-tissue separation. Figure 9 shows the simulated variations of peak SAR (inside muscle layer) with power fed to the MDH designed at 915 MHz which is in direct contact with a bio-model without tumor by taking the composition of bio-model as a parameter and keeping the wave polarization unchanged. It can be observed from Fig. 9 that as input power increases, peak SAR in the muscle layer increases for both bio-models. But for same input power, the value of peak SAR is smaller for the tri-layered skin-fat-muscle model as compared with the homogeneous bio-model. This effect was observed due to the existence of reflections at various interfaces of the tri-layered bio-model.

Simulations were also performed for absolute SAR distributions in tri-layered bio-media (skin, fat, and muscle) without and with embedded tumors (taken one at a time) due to the MDH to which 1 W input power was applied and the results are shown in Figs 10 and 11. Figure 10 shows the simulated variations of absolute SAR distribution in the tri-layered bio-media without and with embedded oval-/irregular-shaped tumors (taken one at a time), along *z*-direction (for $x = y = 0$) whereas Fig. 11 shows the

https://doi.org/10.1017/S1759078718000739 Published online by Cambridge University Press

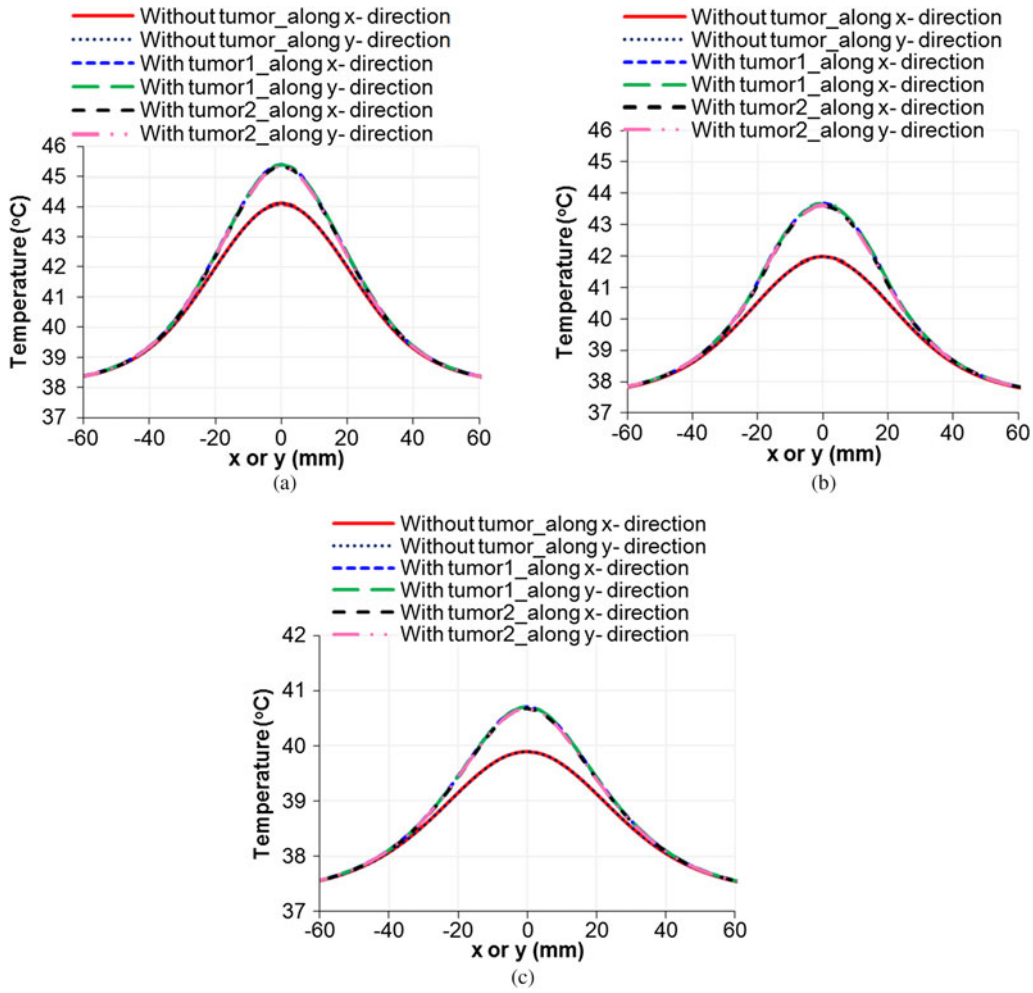

Fig. 15. Simulated temperature distributions inside the tri-layered bio-model without tumor, with embedded tumor1 and with embedded tumor2 along *x*-/*y*-direction ($y/x = 0$) at (a) $z = 5$ mm (b) $z = 17.5$ mm (c) $z = 30$ mm due to the MDH at 915 MHz for optimum input power of 13 W.

variations of absolute SAR distributions in the aforesaid configurations of bio-media along *x*-/*y*-direction due to the MDH. The values of penetration depth and EFS extracted from Figs 10 and 11 are given in Table 6. It can be inferred from Table 6 that very small changes are observed in penetration depth and EFS (in the middle of tumor) due to the presence of a tumor.

Temperature distributions in tri-layered bio-media

The performance of hyperthermia applicator is characterized through temperature distribution in the tissue. The heat generated due to EM energy absorption in the tissue is proportional to SAR. The temperature distribution inside the realistic tri-layered tissue model was evaluated using Pennes' bio-heat equation (BHE) [20].

In order to demonstrate the hyperthermia treatment system, inhomogeneous tri-layered bio-models fed through water-loaded MDH designed at 915 MHz was considered. The thermal simulation was carried out using CST multiphysics simulator software at an initial tissue temperature of 37 °C in which convective heat transfer coefficient between tissue and fluid of water-loaded applicator was assumed to be zero. The simulation provides open thermal boundary conditions at a background temperature of 25 °C. The thermal parameters of bio-models used in the simulation are listed in Table 7.

Figure 12 shows the variations of temperature as a function of depth in the tri-layered bio-model without tumor due to the MDH designed at 915 MHz by taking input power level as a parameter. It can be seen from Fig. 12 that as power fed to the applicator increases, the temperature in the bio-media rises and decreases exponentially with depth inside the bio-media. It can also be inferred from Fig. 12 that for the present MDH antenna, the input power of 13 W was optimum for obtaining the desired hyperthermia temperature range (41–45 °C).

Figure 13 shows the variations of temperature in the biological media with time owing to the MDH designed at 915 MHz for normal bio-model without tumor and the model with embedded irregular tumor (tumor2) by taking depth in the muscle as a parameter. The power fed to the applicator for each bio-model was taken as 13 W. It is noticed that tumor temperature in each case reaches to a higher value as compared with normal tissue temperature (Fig. 13). This would support in effective heating of tumor in the superficial region of the body compared with normal tissue. Further, it can be observed from Fig. 13 that initial rate of rise of temperature is higher at a lower depth in the realistic tri-layered bio-media without and with embedded tumor2. The rate of rise of temperature in each case slows down after 40 min of heating and reaches a steady value after about 50 min of heating at a given depth. The results demonstrate that tissue temperature

https://doi.org/10.1017/S1759078718000739 Published online by Cambridge University Press

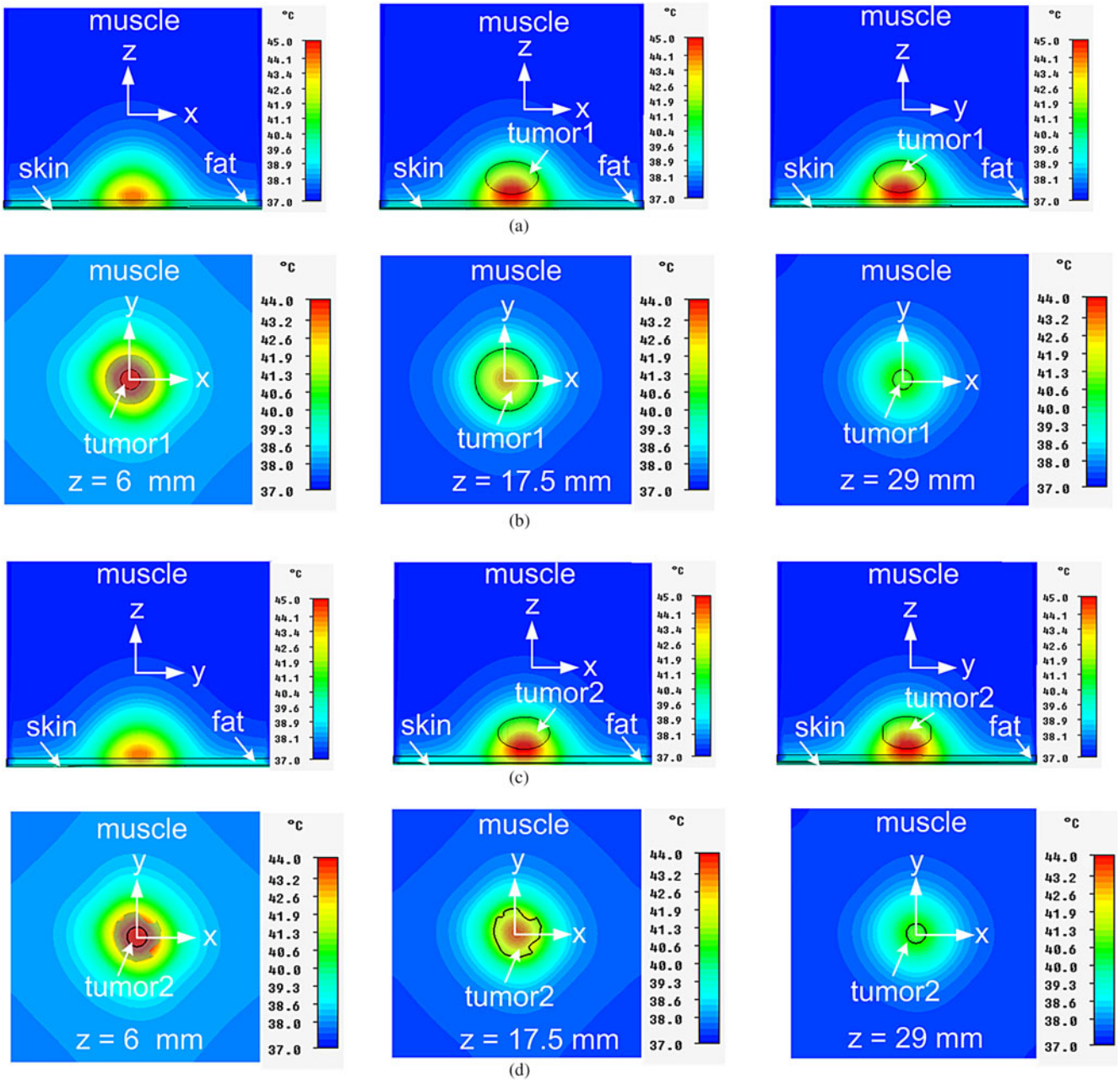

Fig. 16. Temperature distributions inside the realistic tri-layered bio-media due to MDH at 915 MHz for 13 W optimum input power (a) without and with embedded tumor1 in *xz*/*yz* planes for ($y/x = 0$) (b) with embedded tumor1 in *xy*-plane (c) without and with embedded tumor2 in *yz*/*xz* plane(s) for ($x/y = 0$) (d) with embedded tumor2 in *xy*-plane.

approaches saturation after 50 min of heating at a given depth and shows decreasing trend as the depth in the muscle medium increases.

Figure 14 shows the profiles of temperature along *z*-direction respectively, in the tri-layered bio-media without and with embedded tumor (tumor1/tumor2) due to the water-loaded applicator for an optimum input power of 13 W by taking tumor configuration as a parameter. It is clear from Fig. 14 that temperature profiles are similar for different tumor shapes. Moreover, the applicator provides sufficient heat for the tumor embedded in the bio-model (Fig. 14). Further, the depth at which temperature elevation is half of the maximum with respect to initial temperature (=ΔT/2) (derived from Fig. 14 in each case) is given in Table 6. Further, it is observed from Fig. 14 that the presence of tumor of one configuration or another affects to a certain degree the temperature distribution along the depth at the frequency of interest.

Figure 15(a)–15(c) depicts the profiles of temperature distribution in the bio-models without tumor, with embedded tumor1 and embedded tumor2 along *x*-/*y*-direction ($y/x = 0$) at different depths of tumor due to the applicator for optimum input power of 13 W. The results show that the MDH is able to heat whole tumor volume effectively.

Figure 16(a)–16(d) shows the cross-sectional profiles of temperature distribution in the bio-models without and with tumor1 in *xz*/*yz* plane(s) for ($y/x = 0$), with embedded tumor1

https://doi.org/10.1017/S1759078718000739 Published online by Cambridge University Press

in *xy* plane for $z = 6$, 17.5, and 29 mm, without and with embedded tumor2 in *yz*/*xz* plane(s) for ($y/x = 0$) and with embedded tumor2 in *xy*-plane for $z = 6$, 17.5, and 29 mm respectively, owing to the MDH at 915 MHz for 13 W optimized input power. It can be seen from Fig. 16 that desired temperature range (41–45 °C) is maintained in the whole volume of superficial tumors for effective hyperthermia. Symmetrical temperature distributions in the tissue medium due to the applicator can be observed in the transverse *xy*-plane (Figs 16(b) and 16(d)).

Conclusion

The hyperthermia performance of water-loaded MDH terminated in bi-layered/tri-layered tissue media has been investigated theoretically and through simulation at 915 MHz. Theoretical and/or simulated SAR and temperature distributions in the phantom bi-layered (fat, muscle) bio-media/realistic tri-layered bio-media due to the MDH at 915 MHz have been determined. Results achieved through theoretical study indicate that reasonably good impedance matching between the MDH aperture and the bi-layered bio-media has been achieved. Further, as fat thickness increases, reflection at the interface of the MDH aperture and bi-layered bio-media increases. The results obtained through simulation study corroborate the annotation that peak value of SAR in the muscle layer decreases and magnitude of input reflection coefficient increases as fat thickness increases. It can be inferred from the simulation study of temperature distributions in the realistic tri-layered bio-models that the water-loaded MDH designed at 915 MHz with 13 W input power can be used for hyperthermia treatment of irregular-/oval-shaped tumors in superficial abdominal/limb region of the body.

Acknowledgement. Soni Singh is thankful to the Ministry of Human Resource Development, Government of India for providing the financial assistance in the form of teaching assistantship.

References

1. **Chuang H-R** (1997) Numerical computation of fat layer effects on microwave near-field radiation to the abdomen of a full-scale human body model. *IEEE Transactions on Microwave Theory and Techniques* **45**(1), 118–125.
2. **Chou CK *et al.*** (1990) Effects of fat thickness on heating patterns of the microwave applicator MA-151 at 631 and 915 MHz. *International Journal of Radiation Oncology BiologyPhysics* **19**(4), 1067–1070.
3. **Curto S *et al.*** (2009) Compact patch antenna for electromagnetic interaction with human tissue at 434 MHz. *IEEE Transactions on Antennas and Propagation* **57**, 2564–2571.
4. **Lin JC, Kantor G and Ghods A** (1982) A class of new microwave therapeutic applicators. *Radio Science* **17**(5S), 119S–123S.
5. **Van Rhoon GC, Rietveld PJ and Van Der Zee J** (1998) A 433 MHz lucite cone waveguide applicator for superficial hyperthermia. *International Journal of Hyperthermia* **14**(1), 13–27.
6. **Guy AW** (1971) Electromagnetic fields and relative heating patterns due to a rectangular aperture source in direct contact with bilayered biological tissue. *IEEE Transactions on Microwave Theory and Techniques* **19**(2), 214–223.
7. **Maity S, Barman KR and Bhattacharjee S** (2017) Silicon-based technology:circularly polarized microstrip patch antenna at ISM bandwith miniature structure using fractal geometry for biomedical application. *Microwave and Optical Technology Letters* **60**, 93–101.
8. **Bhattacharjee S *et al.*** (2016) Performance enhancement of implantable medical antenna using differential feed technique. *Engineering Science and Technology, an International Journal* **19**, 642–650.
9. **Paulides MM *et al.*** (2013) Simulation techniques in hyperthermia treatment planning. *International Journal of Hyperthermia* **29**(4), 346–357.
10. **Singh S and Singh SP** (2014) Water-loaded metal diagonal horn applicator for hyperthermia. *IET Microwaves,* Antennas & Propagation **9**(8), 814–821.
11. **Singh S and Singh SP** (2015) Theoretical and simulation studies on water-loaded metal diagonal horn antenna for hyperthermia application. *Progress In Electromagnetics Research C* **58**, 105–115.
12. **Gupta RC and Singh SP** (2005) Analysis of the SAR distributions in three-layered bio-media in direct contact with a water-loaded modified box-horn applicator. *IEEE Transactions on Microwave Theory and Techniques* **53**(9), 2665–2671.
13. **Trefna HD *et al.*** (2017) Quality assurance guidelines for superficial hyperthermia clinical trials: I. Clinical requirements. *International Journal of Hyperthermia* **33**(4), 471–482.
14. **CST [MWS]**. [Online]. http://www.cst.com.
15. **Love AW** (1976) *Electromagnetic horn antennas*. New York, NY: IEEE Press.
16. **Compton RT** (1964) The admittance of aperture antenna radiating into lossy media. Antenna Laboratory. OH, Ohio State University, Research Foundation, Columbus.
17. **Harrington RF** (1961) *Time–harmonic Electromagnetic field*. New York, NY: McGraw–Hill, pp. 123–135.
18. **Gabriel C** (1996) *Compilation of the dielectric properties of body tissues at RF and microwave frequencies*. London, TX: Brooks AFB. (Tech. Rep. AL/OE–TR–1996–0037).
19. **Michaelson SM and Lin JC** (1987) *Biological effects and health implications of radiofrequency radiation*. New York, NY: Plenum Press.
20. **Pennes HH** (1948) Analysis of tissue and arterial blood temperatures in the resting human forearm. *Journal of Applied Physiology* **1**, 93–122.
21. **Gong Y and Wang G** (2009) Superficial tumor hyperthermia with flat left-handed metamaterial lens. *Progress In Electromagnetics Research* **98**, 389–405.
22. **Nikawa Y *et al.*** (1986) A direct-contact microwave lens applicator with a microcomputer-controlled heating system for local hyperthermia. *IEEE Transactions on Microwave Theory and Techniques* **34**(5), 626–630.

Soni Singh was born in Deoria, UP, India in 1989. She received the B.Sc. degree in Electronics from DDU Gorakhpur University, India in 2009 and M.Sc. degree in Electronics from Banasthali University, Rajasthan, India in 2011. She completed her Ph.D. work in 2016 from the Department of Electronics Engineering, IIT (BHU), Varanasi, India. She is author or co-author of 11 journal papers and 20 international/national conference papers. Her major research activity includes dielectric loaded metal horn antenna, medical applications of microwaves, and antenna technology.

Bhagirath Sahu received the Bachelor of Engineering (B.E.) degree in Electronics and Communication Engineering from RGPV, Bhopal, India, in 2010, and the M.Tech degree in Electronics Engineering (Microwave Engineering) from Indian Institute of Technology (Banaras Hindu University), Varanasi, India, in 2013. He is currently working towards the Ph.D. degree in Electronics Engineering (Microwave Engineering) from Indian Institute of Technology (Banaras Hindu University), Varanasi, India. He is author or co-author of about 12 Journal papers and 20 international/national conference papers. His research interests include microstrip filters, filtering antennas, dielectric resonator antennas, antennas for wireless/biomedical applications and metamaterials. Mr. Sahu is a student member of the Institute of Electrical and Electronics Engineers (IEEE) Microwave Theory and Techniques Society (MTT-S). He is founder chairperson of IEEE MTT-S Student Branch Chapter (SBC) at IIT (BHU) Varanasi in the Uttar Pradesh (UP) Section, India since May, 2017.

https://doi.org/10.1017/S1759078718000739 Published online by Cambridge University Press

Surya Pal Singh (corresponding author) was born in Mendia, UP, India in 1951. He received the B.Sc. degree in Science, B.Tech. degree in Electronics Engineering, M.Tech. and Ph.D. degrees in Electronics Engineering (Microwave Engineering) from Banaras Hindu University (BHU), Varanasi, India, in 1971, 1976, 1979 and 1989, respectively. He had been employed at Department of Electronics Engineering, IT, BHU (now IIT (BHU)), Varanasi since 1980 and retired as Professor on January 31, 2016. Presently, he is re-employed as Institute Professor in the same institute. He has been Coordinator of the UGC funded CAS program during 2005–2011, and Head of the Department during 2010–2013. He has supervised/co-supervised 12 Ph.D. theses and 64 M.Tech. Dissertation projects. He has authored/co-authored over 190 research papers in international/national journals and conference proceedings. His areas of current research and publications include bio-electromagnetics, microwave antennas, and microwave measurements. Prof. Singh is a Life Senior Member of IEEE, USA and a Life Fellow of IETE, India.

https://doi.org/10.1017/S1759078718000739 Published online by Cambridge University Press